The cyclic unit beneath the UG1 chromitite (UG1FW unit) at RPM Union Section Platinum Mine—Rosetta Stone of the Bushveld Upper Critical Zone?

H. V. EALES, W. J. DE KLERK, A. R. BUTCHER

Department of Geology, Rhodes University, Grahamstown, South Africa

AND

F.J. KRUGER

Bernard Price Institute, University of the Witwatersrand, Johannesburg, South Africa

Abstract

The UG1 Footwall unit is a layered pyroxenite–norite–leuconorite–anorthosite sequence between the Middle Group 4 and Upper Group 1 chromitites of the Upper Critical Zone, and is *c.* 300 m thick at Rustenburg Platinum Mines, Union Section, where it shows an oscillatory fluctuation in whole-rock Mg/(Mg + Fe), Cr/Co, Ni/V and Fe/Ti ratios with stratigraphic height. This permits subdivision into 8 sub-cycles which match a subdivision based on cyclical variations in orthopyroxene and feldspar compositions. Constituent pyroxene grains of pyroxenites, norites and leuconorites alike contain rounded and embayed plagioclase inclusions in abundance. Sr-isotope disequilibrium prevails in some samples between the orthopyroxene and feldspar populations. Chemical and isotopic data support a model of pulsatory injection of limited volumes of a more primitive, mafic liquid into a resident column of depleted residua, from which sodic labradorite and Mg-poor bronzite were crystallizing. The depleted liquid is equated with the supernatant liquid residuum of buried cumulates (Sr_i *c.* 0.7054) and the primitive liquid with magma parental to the UG1–UG2 lineage ($Sr_i \geq 0.7068$). The increase in leucocratic character of the 300 m column, with height, is attributed to the rising of low-density liquids enriched in the components of feldspar during separation of the pyroxenites. Deposition of the UG1 chromitite layers is attributed to mixing of a major influx of primitive liquid with a feldspathic residuum at the top of the UG1 Footwall unit. There is no evidence to indicate the participation of a discrete A-type liquid (Irvine and Sharpe, 1982) in this process.

KEYWORDS: Bushveld complex, magma mixing, chromitite, compositional convection.

Introduction

IN comparison with the Eastern Bushveld Complex, where outcrops of the layered sequence are generally good, the succession in Western Bushveld is not at all well exposed, and, in the case of the Critical Zone, a flat and rather featureless plain veneered by a black turf soil is all that is seen at the surface. Although considerable underground mining activity in the area for the exploitation of the platinum-bearing horizons—Merensky Reef and Upper Group Chromitite Layer 2 (UG2)—has exposed the uppermost parts of the Critical Zone (between the Upper Group Chromitite Layer 1 (UG1) and the Merensky-Bastard Units), relatively little is known about the cumulate sequences below the normal mineable limits, which are only exposed in the tramming and ventilation crosscuts from production shafts.

This paper presents textural and geochemical data pertaining to a suite of samples taken from one such crosscut, which has enabled documentation of a section extending approximately 350 m beneath the UG1 chromitites—including the

Mineralogical Magazine, March 1990, Vol. 54, pp. 23–43

so-called UG1 Footwall Unit (UG1FW)—in the Rustenburg Platinum Mines (R.P.M.) Union Section area, north-western Bushveld Complex. The aim is to build on the existing data base for the Upper Critical Zone and to provide further evidence and support for a model already proposed by Eales *et al.*, (1986, 1988). In this model it is argued that geochemical differences between successive units represent evidence for repeated injections of fresh, primitive magma into a column of partially depleted liquid resident above the crystalline floor of the chamber. The more mafic rocks, constituting the lower parts of cyclic units, are taken to have crystallized from such new inputs of liquid, whereas the more evolved or more leucocratic upper members have crystallized from hybrid liquids resulting from the mixing of the old and the new magmas.

The stratigraphic succession

The Bushveld Complex is broadly divisible into Marginal, Lower, Critical, Main and Upper Zones, the combined thickness of which is some 7000 m in the Western limb. The first appearance of cumulus plagioclase feldspar within the column is used to segregate the ultramafic dunites, harzburgites, pyroxenites and chromitites of the Lower Critical and Lower Zones from rocks of the Upper Critical Zone (harzburgites, pyroxenites, norites, chromitites and minor anorthosites), the Main Zone (gabbronorites and anorthosites) and the Upper Zone (magnetite gabbros, magnetites, and evolved gabbros containing fayalitic olivine and cumulus apatite).

Detailed descriptions of the succession through the Upper Critical Zone in the northwestern part of the complex are available in the literature (Eales, 1987; Eales, *et al.*, 1986, 1988; Viljoen *et al.*, 1986*a,b*), and no more than a summary is necessary here (see Fig. 1). The Bastard and Merensky Units are ostensibly 'complete' cyclic units, comprising ultramafic members (feldspathic pyroxenites, with or without accompanying feldspathic harzburgites) at the base, grading upwards through melanorites, norites and leuconorites to anorthosites at the top. Plagioclase is of intercumulus habit within the ultramafic members, but adopts cumulus habits and becomes more calcic within and above the melanorites of each unit. The Merensky Footwall Unit forms the floor upon which the economically important, P.G.M.-enriched Merensky Reef rests, and may be characterized as a largely leucocratic sequence with trivial development of an ultramafic facies at its base. The Pseudoreef Multicyclic Unit beneath the Footwall Unit is largely an association

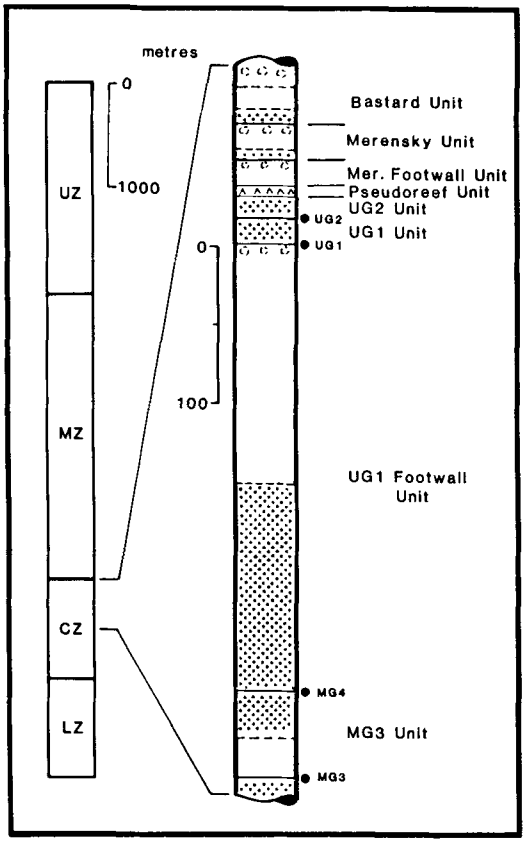

FIG. 1. Generalised stratigraphic succession through Western Bushveld with detail for the Upper Critical Zone at Union Section. Significant chromitite layers at bases of units are indicated by filled circles. Stipple—pyroxenites; unshaded—norites and leuconorites; circles—anorthosites; cone ornament—harzburgite. LZ—Lower Zone; CZ—Critical Zone; MZ—Main Zone; UZ—Upper Zone.

of leuconorites and norites with feldspathic harzburgites (the Pseudoreefs), and is well developed at Amandelbult Section, but reduced to no more than two harzburgite layers at Union Section. The underlying UG2 and UG1 units are composed essentially of feldspathic pyroxenites floored by well developed chromitite layers up to 1 m thick.

The contact between the UG1 and the underlying UG1FW Unit is one of the more spectacular features of the Complex. In some parts of Union Section mine, an upper chromitite layer (50–60 cm thick) is separated from a lower layer (*c.* 30 cm) by *c.* 30 cm of pyroxenite, and this package rests concordantly upon snowy-white anorthosite constituting the top of the UG1FW unit. Elsewhere, the contact shows the same complexities as

are displayed at the well-known Dwars River exposures in the Eastern Bushveld Complex (Figs 196–201, Wager and Brown, 1968). An upper group of regular chromitite layers overlies 3–4 m of anorthosite within which thin chromitite layers (commonly 1–200 mm thick) converge and diverge to yield an anastomosing system. This may in turn give way to an irregular system of contorted, discontinuous stringers, lenses and pods of chromitite. Lenticular chromitite pods with an oblate-spheroid shape, and diameters up to 0.5 m, appear to have subsided within the anorthosite, depressing and disrupting the layering beneath and around the pods (Fig. 2*a*). These structures have been variously attributed to intrusion into the anorthosite of a chromitite-bearing residual magma (Sampson, 1932), intrusion of anorthosite into chromitite (Coertze, 1958), deposition of chromitite accompanied by turbulent mixing with plagioclase crystals (Vermaak, 1976), and emplacement of a chromitite mush as a result of fracturing (Cameron, 1964) or a process akin to that which produces sandstone dykes and sills in sediments (Lee, 1981).

The upper half of the UG1FW unit comprises a leucocratic suite. An upper layer of chromitiferous anorthosite (2–3 m thick) rests upon *c.* 5 m of what is locally known as the 'Streaky Norite', displaying mm-scale layering (Fig. 2*a*). Beneath this is a second couplet of Cr-poor anorthosite and leuconorite resting upon *c.* 130 m of norite alternating with leuconorite and minor pyroxenite. This grades downwards, via some 20 m of pyroxenite alternating with melanorite to a 115 m pyroxenite member floored by the MG4 chromitite. The total thickness of this unit (*c.* 285 m) is thus appreciably greater than that of other cyclic units in the northwestern exposures of the Upper Critical Zone, such as the Merensky and Bastard Units (20–30 m; Eales *et al.*, 1986, 1988). Justification for treating it as a single unit lies in (i) correspondence with the sequence chromitite–pyroxenite–melanorite–norite–leuconorite–anorthosite, characterising cyclic units elsewhere, and (ii) internal coherence of geochemical parameters (described later) which distinguish it from units above and below.

Between the MG4 and MG3 chromitites, the sequence is essentially an upward gradation from norite to pyroxenite, followed by an abrupt transition to anorthosite within the uppermost 1.5 m constituting the immediate footwall to the MG4 chromitite. A similar transition occurs immediately beneath the MG3 chromitite.

Some of the field characteristics of this sequence are implicit in the variations in whole-rock Al_2O_3 and normative minerals shown in Fig. 3. These are (i) the existence of a continuum of compositions between pyroxenite and anorthosite, but with a dominance of pyroxenites (<6.5% Al_2O_3) and norites (11–21% Al_2O_3), (ii) gradations from one horizon to another, as from pyroxenite to norite (160 m to 130 m), pyroxenite to leuconorite (125 m to 94 m) and melanorite to anorthosite (57 m to 8 m), and (iii) gradual but sustained increases in proportions of pyroxenes with stratigraphic height within parts of the sequence, as between 330 m (norite) and 300 m (pyroxenite), or 94 m (leuconorite) and 57 m (melanorite).

Petrography of the UG1 Footwall Unit

The UG1 Footwall Unit comprises orthopyroxene, plagioclase feldspar, clinopyroxene, chromite and magnesian biotite in various modal proportions. Following Eales *et al.* (1986) rocks with <6.5% Al_2O_3 and intercumulus feldspar only are termed pyroxenites; melanorites fall within the range 6.5–11% Al_2O_3, norites 11–21%, and leuconorites 21–28%. In pyroxenites, poikilitic clinopyroxene may form oikocrysts up to 0.5 cm in diameter, enclosing all older phases. Within norites, clinopyroxene may rim orthopyroxene and be optically continuous with exsolved blebs within the latter. Mica is invariably interstitial. Chromite is a rare accessory phase, in contrast with its ubiquitous occurrence in the overlying UG1, UG2, Merensky Footwall and Merensky Units. Only between 210 m and 250 m, and immediately above the MG4 chromite, are traces (*c.* 0.1%) of this phase found.

Grain-size indices plotted in Fig. 3 represent the mean value of the longer intercept of 30–60 orthopyroxene grains intersected, on a rectilinear grid, in each thin section. There is no obvious orientation of grains within the samples examined. A range of 0.63–2.65 mm is displayed. The rocks of finest grain size (0.6–1.25 mm) are pyroxenite adcumulates with well developed 120° triple junctions and low feldspar contents. The overlying noritic rocks are distinctly coarser (1.15–2.65 mm) with poorly developed crystal shapes—at best, a minority of grains are subhedral.

The uppermost 20 m of the unit includes leuconorites and anorthosites. Cumulus orthopyroxene is macroscopically visible in leuconorites ('spotted anorthosites') but true anorthosites with >28% Al_2O_3 bear only trivial amounts of intercumulus pyroxene. A poikilitic habit adopted by pyroxene yields 'mottled anorthosite'. Grain size of these rocks is normally 0.5–3 mm, and preferred orientation of feldspar laths, parallel to the layering, may be adopted.

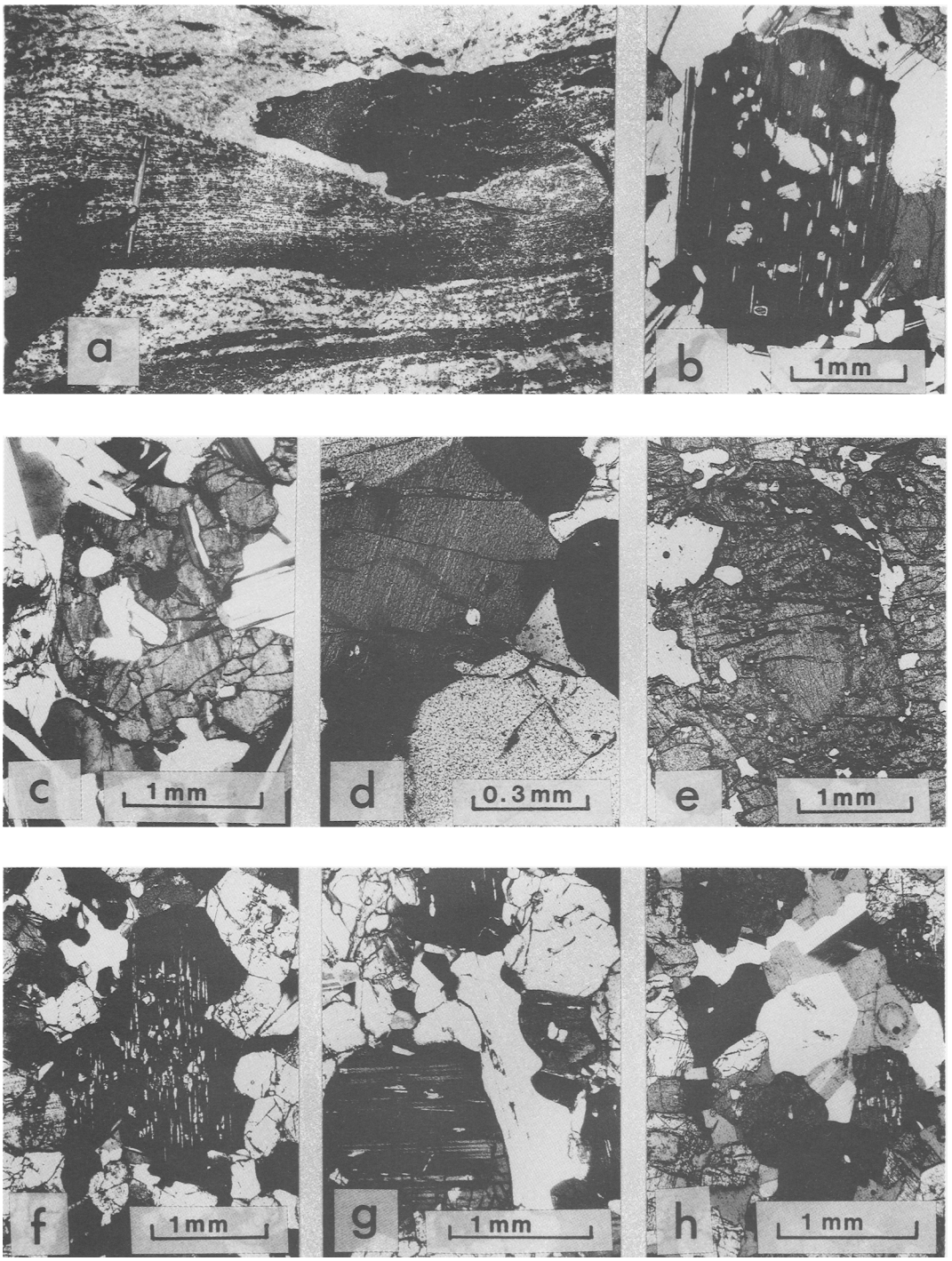
a
b
1mm
c
1mm
d
0.3mm
e
1mm
f
1mm
g
1mm
h
1 mm

A significant and distinctive feature of the sampled section of the UG1FW unit is the abundance of small plagioclase inclusions within pyroxenes of norites (Fig. 2 *b–c*) and pyroxenites (Fig. 2 *d–f*) alike. These inclusions are commonly 0.02–0.25 mm in diameter, and spheroidal, ovoid or irregularly embayed. Some form clusters. Their frequency is variable, up to 20 particles being quite commonly seen per host grain, but no sample is free of them. Their distribution and orientation are random within their hosts. Their shapes are wholly atypical of cumulus plagioclase within noritic rocks, and the intergrowth is in no sense comparable with ophitic texture or of the fabric adopted by intercumulus pyroxenes within anorthosites. A further variety of plagioclase occurs as sparse laths up to 1.5 mm in length (Fig. 2*g*) or clusters up to 2.5 mm (Fig. 2*h*) embedded in some pyroxenites. Isotopic evidence, presented later, establishes beyond question that these are xenocrysts. In summary, therefore, these pyroxenites are characterised by the presence of intragranular, intergranular, and intercumulus varieties of plagioclase. We interpret the texture as unequivocal evidence for nucleation of pyroxenes within melts containing partially resorbed, earlier-generation feldspar. In the case of norites, plagioclase occurs both as partially resorbed inclusions within orthopyroxene host grains, and as a cumulus phase.

Mineral compositions of feldspars and pyroxenes in the UG1FW unit

Plagioclase feldspar. Microprobe analyses of the cores of 407 feldspar grains, summarized in Fig. 4, show that the range of composition is $An_{57–85}$. Neither the spheroidal inclusions within orthopyroxene nor grains surrounding pyroxenes constitute a discrete, identifiable population, but some bias is shown insofar as in 20 samples out of 25 (Fig. 4) the more sodic average compositions are yielded by the inclusions. It is also evident that inclusions and non-included feldspar do not vary independently in composition—samples with notably sodic inclusions show the surrounding grains shifted also to more sodic compositions.

The statement of Eales *et al.* (1986, 1988) that feldspar of anorthosites and norites at the tops of cyclic units are more calcic than both cumulus and intercumulus species in underlying rocks, is equally valid here (see Fig. 5). Mean compositions of feldspar cores are $An_{76.5–78.5}$ within the uppermost 25 m of the unit, and $An_{73.5–75.6}$ within underlying norites. Intercumulus grains of pyroxenites are commonly a further 5–10% richer in *ab* molecule.

Fig. 5 displays the compositional trends followed, respectively, by plagioclase included by, and that external to, orthopyroxene. The sympathetic variation established in Fig. 4 is seen to be followed at all stratigraphic levels, and a clear cyclicity is apparent. Within pyroxenites, subcycles show an upward decline of anorthite content, but above the level where cumulus feldspar enters the paragenesis (at 150 m) the trends followed by felsic and mafic phases vary sympathetically. A narrow outer rim may encircle each inclusion. At the base of cycles, where feldspars are calcic, this rim displays reversed zoning, but where more sodic compositions dominate at higher levels, zoning is either of normal type, or absent.

The origin of the inclusions is of critical importance in interpreting the UG1FW unit. The following possibilities exist: (*a*) inclusions are the crystallization products of a paragenetic sequence inverted by spatial shifts of primary phase volumes, under the influence of pressure, f_{O2} or concentration of volatiles, (*b*) inclusions represent feldspar nucleated within a bottom layer enriched in the components of feldspar, following on *in situ* bottom growth of pyroxenites upon the floor, (*c*) inclusions represent undigested remnants of fragmented or eroded, older, anorthositic or noritic layers, or (*d*) inclusions depict partial crystallization of residual melts saturated in feldspar, prior to their re-heating and mixing with later pulses of more primitive, mafic liquid.

FIG. 2. (*a*) Chromitite pod (black, upper right) fringed by anorthosite (white) disrupting and truncating cm-scale layering of uppermost norite in footwall of UG1 chromitite layer in Union Section Mine. (*b*) Bronzite grain hosting numerous ovoid and embayed plagioclase inclusions in leuconorite (Sample S-16). Vertical streaks are exsolved clinopyroxene. (*c*) Bronzite grain in norite (S-27) where feldspar inclusions retain vestiges of lath shapes, typical of upper parts of sub-cycles. (*d*) Pyroxenite adcumulate (S-43) showing advanced resorption of relict plagioclase feldspar. Inclusions are small and, in adcumulates, single inclusions may indent two contiguous bronzite grains. (*e*) Unusual type of zoned bronzite grain with clear core surrounded by mantle containing *c.* 80 partially resorbed feldspar inclusions of various sizes (pyroxenite S-37; 1 nicol). (*f*) Orthocumulus pyroxenite showing typical high density of plagioclase inclusions and exsolved clinopyroxene lamellae in core of bronzite grains, surrounded by clear mantle devoid of inclusions (S-41). (*g*) Pyroxenite (S-40) enclosing cumulus feldspar crystal (white, vertical orientation, right side of frame) and (*h*) cluster of cumulus feldspar grains (centre to upper right) yielding Sr-isotope signatures different to each other and to pyroxene fraction.

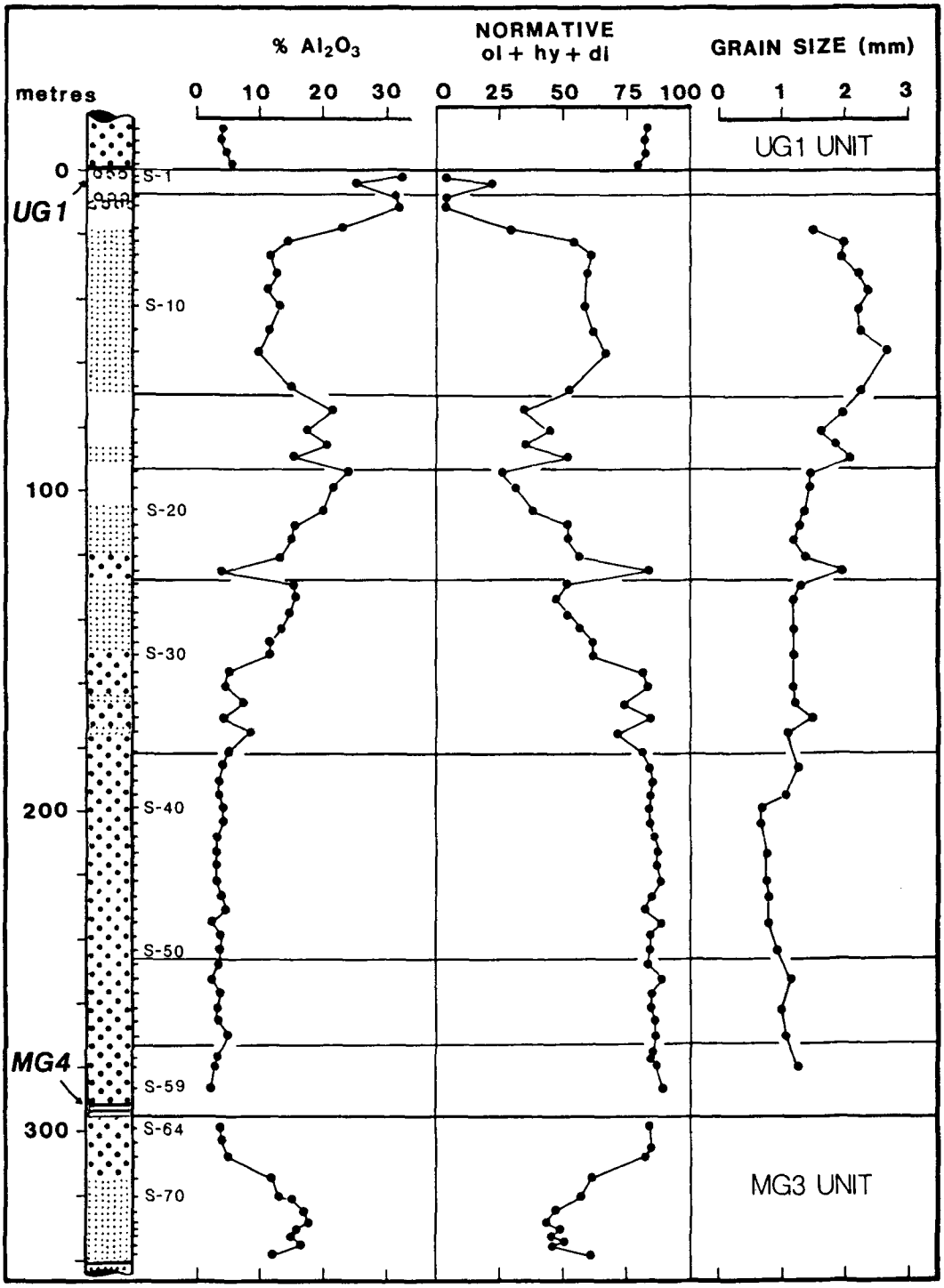

FIG. 3. Variations in wt.% Al_2O_3, normative $ol + hy + di$, and grain size of orthopyroxene through the MG3, UG1FW and base of UG1 units. Coarse stipple—pyroxenites; fine stipple—norites; unshaded—leuconorites; circles—anorthosites; heavy lines—chromitites. Sample positions are shown as S-1 to S-77. Subdivisions of UG1FW unit are based on data presented later (see Fig. 5).

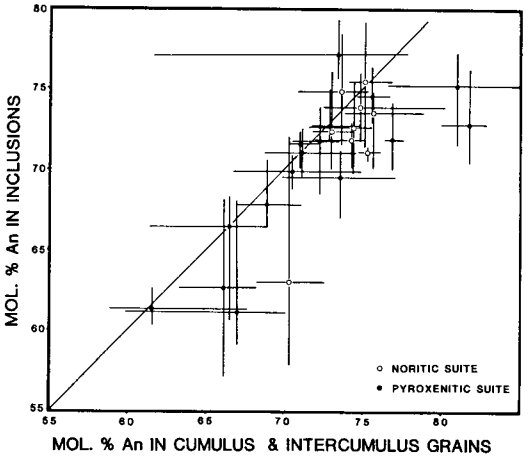

FIG. 4. Compositions (by microprobe analysis) of cores of partially resorbed plagioclase inclusions within orthopyroxene hosts, plotted against compositions of intercumulus and cumulus plagioclase grains in same sample. Bars represent apparent range in composition.

Alternatives (*a*) and (*b*) above ignore the variations in Sr-isotope data (described later) which argue against the texture arising merely out of aberrations in the crystallization of single liquids. Alternatives (*c*) and (*d*) are acceptable *prima facie* models, as they would accommodate the isotopic data, the rounded or embayed habit of the inclusions, and their encapsulation by orthopyroxenes. Inherent properties of the feldspar lattice render volume diffusion and compositional readjustment sluggish processes (Smith, 1974), but optimum conditions for the modification of grain compositions would be yielded by the small size of the inclusions, and super-liquidus conditions implied by resorption. Consequently, the present composition of the inclusions is probably not definitive of provenance, and the sympathetic variations in composition of feldspar inclusions and intercumulus feldspars are attributed to reaction between the inclusions and surrounding liquid.

Orthopyroxenes. 403 microprobe analyses show (Fig. 5) that orthopyroxenes of the UG1FW Unit do not follow the normal evolutionary sequence of magnesian species at the base of a unit giving way to Fe-enriched species towards the top (Eales *et al.*, 1986, 1988). The pattern is one of cyclical variations between a minimum $Mg/(Mg+Fe^2)$ atomic ratio (hereafter abbreviated to MMF ratio) of 0.783 and a maximum value of *c.*0.83. The mean MMF ratio in norites is 0.800 ± 0.007, and 0.794 ± 0.007 in the underlying pyroxenites. Zonal decline in MMF ratios towards crystal margins is muted in norites, never exceeding 1%; significant reversed zoning is absent in norites but not uncommon in pyroxenites. Cr_2O_3 levels in orthopyroxene (Fig. 5) increase from 0.25% at the 180 m level to 0.43% near the top of the norite column. The average in noritic pyroxenes is $0.347 \pm 0.043\%$, and $0.310 \pm 0.028\%$ in pyroxenites. Zonal decline in Cr towards crystal margins is evident in most cases. Absolute Cr-depletion, upward increase in MMF ratios and Cr levels, and good correspondence between MMF ratios and Cr levels in orthopyroxenes thus characterise the major part of the unit.

Fig. 6 shows a plot of Cr_2O_3 against MMF ratios for all samples of the UG1FW unit, together with data points for the Upper Group Chromitite 2 (UG2) pyroxenite and a section above the Lower Group Chromitite Layer 6 (LG6) for which abundant microprobe data are presently available. No discontinuity in trend is apparent. Irrespective of whether the trend is due to fractionation, or crystallization from hybridized liquids, Figs. 5–6 emphasize the anomalous increase in both Cr and Mg through the norites, towards the top of the unit.

A significant drop in MMF ratio to 0.62 and Cr_2O_3 levels averaging 0.02% occurs within the first anorthosite capping the noritic sequence (sub-cycle 7, Fig. 5). This follows the trends typifying anorthosites of the Merensky Footwall, Merensky and Bastard Units (Eales *et al,* 1986). The uppermost leuconorite–anorthosite couplet is, however, remarkable in that MMF ratios are uniquely high (0.82 and 0.85, respectively; see Fig. 5) while Cr_2O_3 in orthopyroxene exceeds 0.5% in the leuconorite and 0.25% in the anorthosite. The uppermost leuconorite is thus anomalously Cr-rich but contains no accessory chromite; the overlying anorthosite contains chromite as a major modal phase. We suggest that this is a contamination effect heralding the development of the overlying Cr-rich UG1 unit.

Whole-rock chemical data

All samples shown in Figs. 3 and 5 have been analysed for major and eleven trace elements. Representative data are presented in Table 1. Whole-rock Al_2O_3 levels (Fig. 3) provide a measure of normative plagioclase in norites and pyroxenites, where $or+ab+an = 3.03\ Al_2O_3 + 0.73$ (correlation coefficient 0.9996, $n = 56$ samples) but over-estimate normative plagioclase in anorthosites where feldspars are more anorthitic. The ratios MMF, Ni/V, Cr/Co and FeO/TiO_2 plotted in Fig. 5 utilise a dividend of higher, and divisor of lower, bulk distribution coefficient and

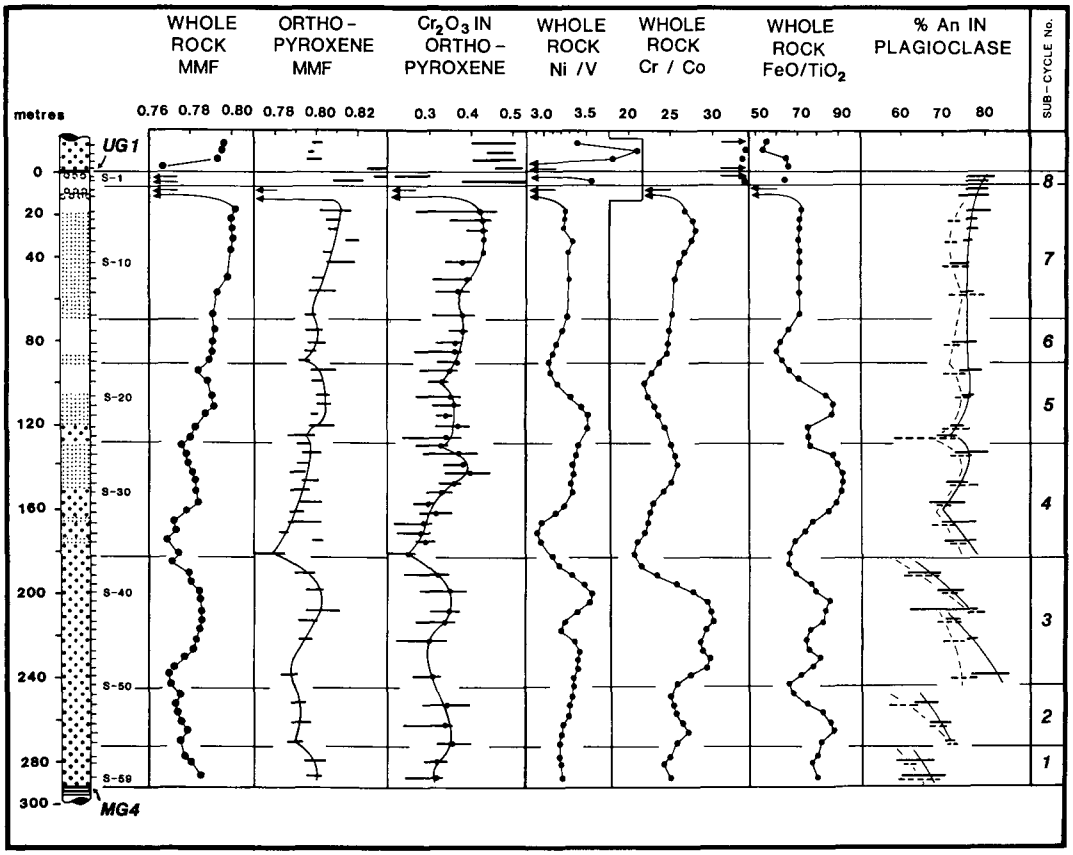

FIG. 5. Compositional trends through UG1FW and base of UG1 units. Whole-rock data smoothed in part by employing three-point moving averages. Bars indicate range of compositions found by microprobe analysis of orthopyroxenes (cores and margins; 403 analyses) and plagioclase feldspars (cores only; 407 analyses). Standard deviation yielded by multiple analyses of single grains was 0.30% An for plagioclase, and 0.002 and 0.019% for MMF and Cr_2O_3, respectively, in orthopyroxene. Filled circles on bars indicate average Cr_2O_3 levels in orthopyroxene cores. For plagioclase, solid bars indicate cumulus and intercumulus grains; dashed bars indicate partially resorbed inclusions. Arrows indicate data points off scale.

accordingly measure the chemical 'primitiveness' of the rock.

The sequence extending for 350 m beneath the UG1 chromitite displays the following features. (*a*) The most evolved rock in terms of MMF ratios is the lower of the two anorthosites within the uppermost 20 m but this ratio is decoupled from feldspar compositions, insofar as the most calcic plagioclase occurs in anorthosites. (*b*) There is no simple trend of cryptic variations within the column beneath the anorthosite roof. The highest (most primitive) MMF ratios are encountered immediately beneath the leucocratic roof, and the lowest at 50 m and 120 m above the MG4 chromitite. (*c*) Variations in Al_2O_3 show that total feldspar may either increase (160–130 m; 125–94 m; 57–0 m in Fig. 2) or decrease (335–30 m; 94–57 m) with height within the section. (*d*) Chemical trends through the Footwall, Merensky and Bastard Units in the northwestern limb of the complex display a saw-tooth pattern (Eales *et al.*, 1986, 1988) because rocks with primitive chemical signatures at the base of units abruptly overlie more evolved rocks at the top of previous cycles. No such pattern exists within the sub-cycles of the UG1FW unit; it is, rather, one of superimposed partial or complete sub-cycles showing a gradual increase in primitive character, followed by gradual decline. Eight such sub-cycles are identified in Figs 2 and 5. Sub-cycles 2–5 are ostensibly complete, with the rise and fall in MMF ratios (whole-rock and microprobe data) being matched to varying degrees of perfection by trends in Ni/V, Cr/Co and FeO/TiO_2 ratios, and Cr_2O_3 levels in

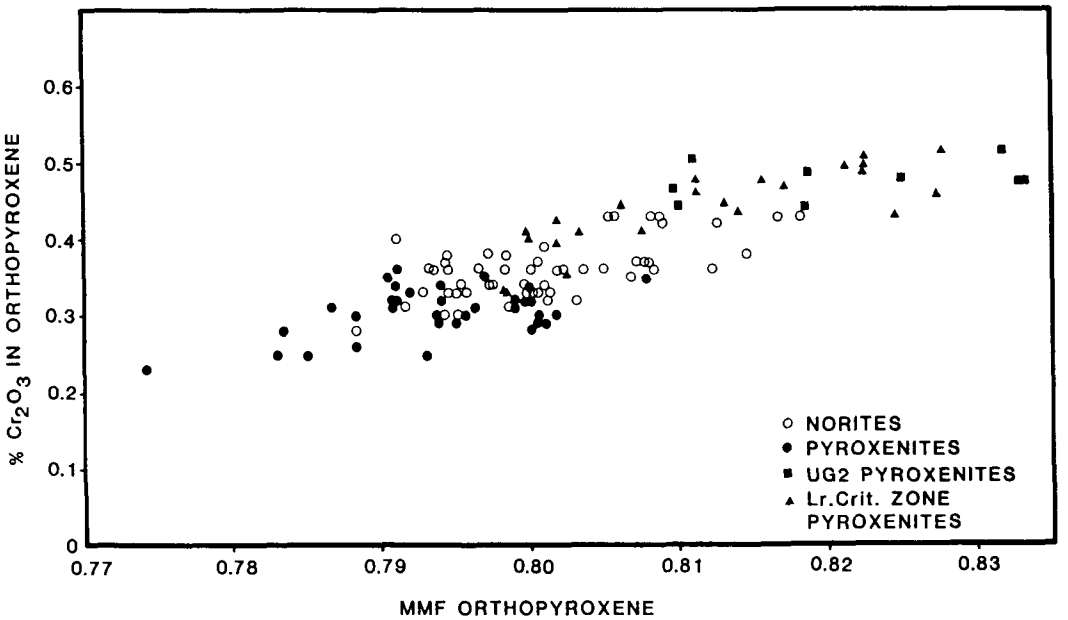

FIG. 6. Cr_2O_3 levels in orthopyroxenes at Union Section, based on averages compiled for UG1FW unit (403 analyses), UG2 unit (220 analyses) and 80 m section above LG6 chromitite of Lower Critical Zone (93 analyses by B. Teigler).

orthopyroxene. This subdivision of the UG1FW unit conforms with that indicated by cyclic variations in feldspar compositions described earlier, but Ni/V, Cr/Co and FeO/TiO_2 ratios, and feldspar data, suggest that sub-cycle 3 is composite. (*e*) Justification for treating the entire sequence between the MG4 and UG1 chromitites as a single unit, despite its great thickness of 285 m, is provided in Fig. 7. Here, the plotting of Sr against V yields a single regression line (Sr = 483.5–2.604 V; corr. coeff. = −0.995; n = 54 samples) which is significantly different to that for samples between the MG3 and MG4 chromitites (Sr = 443–2.743 V). As similar plots of Sr against Al_2O_3 fail to segregate these populations, it is clear that the discrete regression lines in Fig. 7 arise out of relative V-depletion below the MG4 chromitite. Marked inflections in trends of Ni/V and Cr/Co ratios also occur across the MG4 chromitite horizon.

Sr-isotope data

Variations of unexpected magnitude in $^{87}Sr/^{86}Sr$ initial (Sr_i) ratios of four samples were established during an early, exploratory survey, and this led to completion of a further 34 determinations. All results are given in Table 2, incorporating whole-rock and mineral-separate data.

Fig. 8 shows the frequency distribution of Sr_i ratios within the full range from 0.7056 to 0.7075; 60% of values lie between 0.7058 and 0.7064. There is no clear distinction between values for pyroxenites and members of the noritic suite (the subsidiary peak at 0.7070–0.7075 is yielded by five determinations of the isotopically discrete sample S-40). The data are also plotted in Fig. 9 against stratigraphic height, together with unpublished data for the Lower Critical zone and the MG3, UG1 and UG2 units, and published data for the Footwall, Merensky and Bastard units (Eales *et al.*, 1986; Kruger, 1988). Variations with stratigraphic height are seen to approximate a trend of regular increase through the noritic suite, but to follow a non-systematic and unpredictable pattern in the pyroxenites.

Where whole-rock and mineral-separate determinations are available, agreement is good in some samples (S-38 and S-43) but significantly different in others (S-40 and S-49). Results for sample S-40 are instructive. This is a bronzitite, with patchy development of adcumulus texture, analysing 4.4% Al_2O_3 (14% normative plagioclase). Bronzite grains bear spheroidal and embayed feldspar inclusions in the size range 20–125 μm,

TABLE 1 Representative Analyses of Rocks in UG1FW Unit

	1	2	3	4	5	6
SiO_2	54.56	54.36	52.68	52.06	50.67	49.28
TiO_2	0.14	0.16	0.11	0.08	0.05	0.03
Al_2O_3	3.52	3.57	11.75	14.81	23.09	31.81
Fe_2O_3	1.14	1.20	0.78	0.72	0.37	0.08
FeO	11.39	12.00	7.77	7.21	3.67	0.81
MnO	0.25	0.29	0.17	0.16	0.07	0.02
MgO	25.40	24.82	19.14	15.27	8.64	0.83
CaO	3.23	3.18	6.31	8.17	11.57	14.83
Na_2O	0.35	0.38	1.14	1.46	1.79	2.19
K_2O	tr.	0.03	0.13	0.05	0.08	0.11
P_2O_5	0.02	0.01	0.02	0.01	tr.	0.01
Rb	<1	1.9	1.2	1.9	<1	1.7
Sr	41	40	178	223	336	468
Y	3.4	4.7	3.0	2.9	<1	<1
Zr	3.2	7.5	5.6	3.2	<1	<1
Co	105	106	75	64	36	7
Cr	3030	2820	2005	1665	957	48
V	175	173	118	101	54	11
Sc	34	34	23	22	11	9
Ni	572	569	404	339	175	14
Cu	11	15	12	12	11	8
Zn	90	100	62	56	28	11

1. Average of 5 more primitive pyroxenites (S41 - S45).
2. Average of 6 less primitive pyroxenites (S48 - S53).
3. Average of 6 norites near top of unit (S7 - S12).
4. Average of 4 norites at base of noritic suite (S25 - S28).
5. Leuconorite, 18m below top of unit (S5).
6. Average of 2 anorthosites, 8 - 12 m below top of unit (S3-S4).

Major-element data normalised to 100%, L.O.I.- and H_2O-free. Ratio Fe_2O_3/FeO of 0.1 assumed. Trace-element data in ppm.

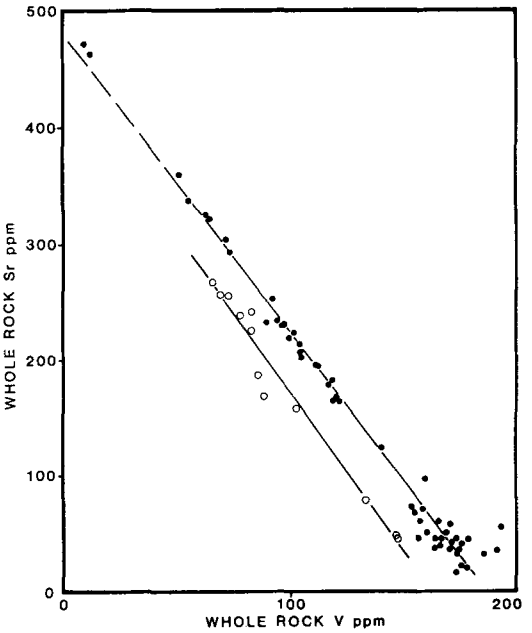

FIG. 7. Plot of whole-rock levels of Sr *vs.* V, to illustrate consistent difference between UG1FW unit (filled circles) and underlying MG3 unit (unfilled circles).

while intercumulus feldspar forms patches up to 0.5 mm. Sparse crystals of apparently cumulus or xenocrystic feldspar up to 1.5 mm long are entangled with the orthopyroxene (Fig. 2 *g–h*). The average of two whole-rock Sr_i ratios is 0.7072 ± 2, within error of the average of two values returned for the orthopyroxene fraction. Values for plagioclase are 0.7061 ± 2 and 0.7075 ± 2, respectively, for two xenocrysts hand-picked from the sample, and 0.7065 ± 2 for a composite plagioclase fraction that should contain all three textural types.

From this it is clear that isotopic disequilibrium may prevail between the phases in some samples, but not in others. Observation suggests that isotopic disequilibrium is maintained where the feldspars are large grains, whereas isotopic and major-element compositional equilibrium with liquid are approached when all inclusions are small. Particularly significant is the confirmation that the feldspar population is a mixed one. Further research is necessary to establish whether this is a general property of the Bushveld complex, as predicted by Eales *et al.* (1986) and Eales (1987).

Plagioclase mineral separates average *c.* 500ppm Sr (Table 2), and orthopyroxenes 3.5–6.5ppm Sr, with no guarantee that, even in −250 mesh fractions, all plagioclase inclusions have been removed. Mass balance calculations using whole-rock Al_2O_3 levels, and Al_2O_3 levels in orthopyroxenes from microprobe analysis, show that even in the more extreme adcumulates, >90% of the total Sr is resident in the plagioclase. The Sr-isotope signature is thus dominated by the feldspar fraction, and the effects of even small amounts of feldspar, not in equilibrium with the host rock, will be pronounced in pyroxenites. This accounts for the contrast between the irregular fluctuations displayed by the feldspar-poor pyroxenitic suite, and more regular trends in the norite suite, illustrated in Fig. 9. It is to be noted that the irregular fluctuations persist into the MG3 unit.

A model involving mixing of liquids, indicated by other geochemical data presented earlier, receives some support from the isotopic data, despite the potentially confusing effects arising

TABLE 2

Isotopic Data

Number	Description	Rb	Sr	$^{87}Rb/^{86}Sr$	$^{87}Sr/^{86}Sr_p$	Sr_i
232/22	Bastard Anorth.	4.95	335.0	0.0427	0.70906 ± 8	0.7078 ± 1
235/3	Bastard Norite	0.47	139.0	0.0098	0.70794 ± 8	0.7076 ± 1
235/6	Bastard Pyrox.	6.42	53.7	0.3462	0.71748 ± 6	0.7073 ± 2
235/8	Merensky Anorth.	5.23	395.0	0.0383	0.70854 ± 6	0.7074 ± 1
235/11	Merensky Norite	1.96	373.0	0.0152	0.70771 ± 8	0.7073 ± 1
235/14	Merensky Pyrox.	3.82	57.7	0.2098	0.71309 ± 6	0.7069 ± 1
235/15a	Merensky Reef	3.69	65.47	0.1631	0.71121 ± 6	0.7064 ± 1
235/18	Footwall Norite	1.77	455.6	0.0112	0.70677 ± 8	0.7064 ± 1
235/21	Footwall Norite	1.61	390.8	0.0119	0.70677 ± 8	0.7064 ± 1
235/23	Footwall Norite	1.09	176.0	0.0179	0.70685 ± 8	0.7063 ± 1
235/25	Pseudoreef Harz.	6.03	543.0	0.0321	0.70710 ± 2	0.7062 ± 1
235/29	UG2 Pyroxenite	8.94	69.2	0.3742	0.71802 ± 6	0.7070 ± 2
235/29	Repeat	9.19	71.0	0.3749	0.71783 ± 7	0.7068 ± 2
235/30	UG2 Pyroxenite	3.69	62.9	0.1698	0.71192 ± 1	0.7069 ± 1
235/31	UG2 Pyroxenite	0.74	72.8	0.0294	0.70719 ± 7	0.7063 ± 1
H235/8	UG2 Chr. Matrix	12.4	372.0	0.0965	0.70958 ± 1	0.7067 ± 1
H235/8	Repeat	13.4	386.0	0.1005	0.70974 ± 2	0.7068 ± 1
235/34	UG1 Proxenite	5.92	61.9	0.2769	0.71453 ± 7	0.7064 ± 2
235/35	UG1 Pyroxenite	6.31	52.2	0.3500	0.71665 ± 1	0.7063 ± 2
235/37	UG1 Pyroxenite	0.504	66.6	0.0219	0.70732 ± 7	0.7067 ± 1
235/39	UG1FW Leuconorite	0.88	413.0	0.0062	0.70647 ± 6	0.7063 ± 1
S-9	UG1FW Norite	0.76	163.0	0.0135	0.70656 ± 1	0.7062 ± 1
S-13	UG1FW Norite	0.84	190.0	0.0128	0.70643 ± 6	0.7061 ± 1
S-19	UG1FW Leuconorite	1.27	326.0	0.0113	0.70644 ± 5	0.7061 ± 1
S-23	UG1FW Norite	1.30	198.0	0.0190	0.70665 ± 3	0.7061 ± 1
S-25	UG1FW Norite	1.16	227.0	0.0148	0.70637 ± 2	0.7059 ± 1
S-30	UG1FW Norite	0.81	174.0	0.0135	0.70615 ± 1	0.7058 ± 1
S-33	UG1FW Melanorite	0.812	97.2	0.0242	0.70671 ± 6	0.7060 ± 1
S-35	UG1FW Melanorite	1.07	125.0	0.0248	0.70685 ± 1	0.7061 ± 1
S-36	UG1FW Pyroxenite	1.57	70.30	0.0646	0.70811 ± 3	0.7062 ± 1
S-38	UG1FW Pyroxenite	0.406	47.6	0.0247	0.70665 ± 1	0.7059 ± 1
S-38	UG1FW Pyrox.(Plg)	1.63	498.0	0.0095	0.70624 ± 1	0.7060 ± 1
S-38	UG1FW Pyrox.(Opx)	0.153	6.07	0.0729	0.70808 ± 3	0.7059 ± 1
S-40	UG1FW Pyroxenite	0.335	70.9	0.0137	0.70770 ± 5	0.7073 ± 1
S-40	Repeat	0.332	75.0	0.0128	0.70760 ± 1	0.7072 ± 1
S-40	UG1FW (Opx -125#)	0.087	6.59	0.0382	0.70845 ± 2	0.7073 ± 1
S-40	UG1FW (Opx +125#)	0.067	6.55	0.0296	0.70801 ± 2	0.7071 ± 1
S-40	UG1FW (Plg)	0.45	513.0	0.0025	0.70655 ± 1	0.7065 ± 1
S-40	UG1FW (Plg Xen.1)	0.828	464.0	0.0052	0.70624 ± 2	0.7061 ± 1
S-40	UG1FW (Plg Xen.2)	0.366	453.0	0.0023	0.70754 ± 2	0.7075 ± 1
S-43	UG1FW Pyroxenite	0.306	37.7	0.0235	0.70681 ± 1	0.7061 ± 1
S-43	UG1FW (Plg)	1.09	513.0	0.0061	0.70630 ± 1	0.7061 ± 1
S-49	UG1FW Pyroxenite	1.14	44.6	0.0740	0.70792 ± 6	0.7057 ± 1
S-49	UG1FW (Plg)	3.79	573.0	0.0191	0.70660 ± 2	0.7060 ± 1
S-54	UG1FW Pyroxenite	1.51	39.4	0.1109	0.70894 ± 8	0.7057 ± 1
S-58	UG1FW Pyroxenite	0.596	36.8	0.0469	0.70756 ± 4	0.7062 ± 1
S-58	Repeat	0.592	37.0	0.0463	0.70768 ± 8	0.7063 ± 1
S-62d	MG3 Norite	0.854	131.0	0.0189	0.70645 ± 1	0.7059 ± 1
S-66	MG3 Pyroxenite	0.563	78.5	0.0207	0.70684 ± 1	0.7062 ± 1
S-68	MG3 Norite	2.13	337.0	0.0183	0.70754 ± 1	0.7070 ± 1
S-71	MG3 Norite	0.784	254.0	0.0089	0.70629 ± 1	0.7060 ± 1
S-78b	MG2 Leuconorite	4.28	406.0	0.0305	0.70649 ± 1	0.7056 ± 1
Lower Critical Zone NG1 Borehole						
NG1-25	Pyroxenite	2.38	34.8	0.1979	0.71142 ± 3	0.7056 ± 1
NG1-49.75	Pyroxenite	1.76	31.9	0.1597	0.71024 ± 2	0.7055 ± 1
NG1-152.2	Pyroxenite	1.97	18.4	0.3099	0.71404 ± 1	0.7049 ± 2
NG1-163.27	Pyroxenite	2.71	39.6	0.1981	0.71110 ± 2	0.7052 ± 1
NG1-204.50	Pyroxenite	2.80	46.5	0.1743	0.71041 ± 1	0.7053 ± 1

Whole-rock and mineral separate Rb-Sr isotopic data for a 600m-section beneath the Bastard Unit. Data are plotted in Fig. 9 against stratigraphic height. Rb and Sr in ppm $^{87}Sr/^{86}Sr_p$ is present-day $^{87}Sr/^{86}Sr$ recovered from spiked sample; uncertainty is 2 standard errors of the mean. Sr_i is initial $^{87}Sr/^{86}Sr$ calculated for an age of 2050 million years; errors are given at the 1σ level. See appendix for further details. NG1 samples refer to a deep borehole drilled in the footwall of RPM Union Section Mine.

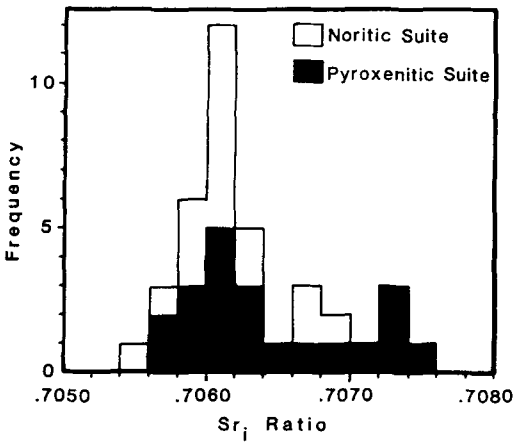

FIG. 8. Histogram showing frequency of occurrence of Sr_i ratios returned by 38 analyses of whole-rock samples and mineral separates, UG1FW, UG1 and UG2 units.

out of fractionation, compositional convection and isotopic disequilibrium. Fig. 10 displays the correlation between MMF ratios of orthopyroxenes (as determined by microprobe analysis) and Sr_i ratios. Included also are four data points representing Lower Critical Zone pyroxenites above the LG6 chromite layer at Union Section (Teigler, 1989) and six olivine- and chromite-poor UG1 and UG2 pyroxenites overlying the UG1FW unit. Despite scattering, 87% of UG1FW unit, and the six UG1–UG2 data points, define a regression line $MMF_{opx} = 20.758\ Sr_i - 13.8542$ (corr. coeff. 0.914). A plot of Cr_2O_3 levels in orthopyroxene against Sr_i ratios yields a distribution similar to that of Fig. 10, but with more scatter.

Fig. 10 therefore supports a model in which crystallization of Mg- and Cr-rich cumulates lower in the stratigraphic section (Sr_i *c.* 0.7054) generated an Fe-enriched, Cr-poor supernatant liquid residuum maintaining the same isotopic signature. This was then mixed in different proportions with liquid similar to that which was parental to the overlying UG1 and UG2 units (Mg- and Cr-enriched, Sr_i 0.7067–0.7070) during deposition of the UG1FW unit.

Sample S-36 is significantly displaced below the regression line of Fig. 10. This is almost certainly a result of crystal fractionation, as the sample represents the top of the pyroxenite suite immediately beneath the first melanorite layer, where the lowest values of MMF, Ni/V, Cr/Co and Fe/Ti in the UG1FW unit are encountered. Sample S-40 is wholly anomalous; the presence within it of xenocrystic plagioclase with Sr_i ratios of 0.7075

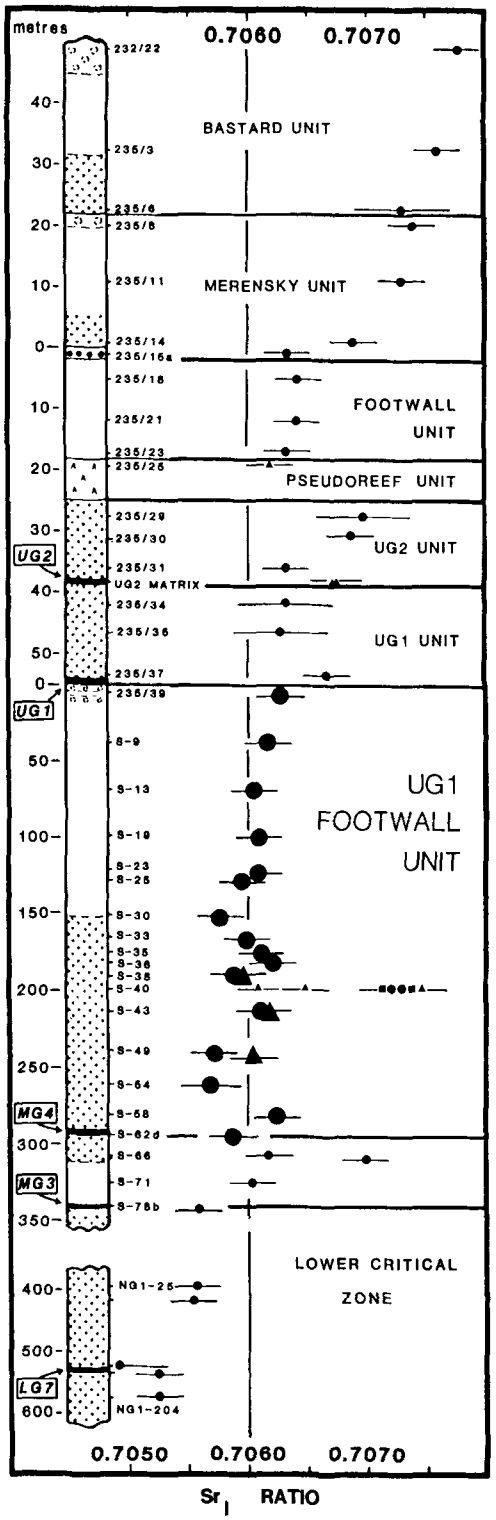

raises several alternative explanations, but these are little better than speculation at present.

Summary of the more relevant diagnostic data

Seven features of particular genetic significance may be isolated after excision of the finer details in the foregoing presentation.

(*a*) The UG1FW Footwall Unit is of exceptional thickness (285 m), but is geochemically coherent, and distinguishable from the units above and beneath it. Pyroxenite overlying chromitite is dominant within the lowermost 135 m, while norites of varying colour index constitute the succeeding 130 m section. The unit is capped by a lower leuconorite–anorthosite couplet displaying evolved attributes (low MMF ratios and Cr levels in orthopyroxene), which is overlain by a second leuconorite–anorthosite couplet in which MMF ratios of orthopyroxenes are higher than in any underlying member of the unit (Fig. 5) and in which Cr contents are anomalously high for rocks of leucocratic affinity. Chromite appears in abundance within the uppermost anorthosite, which is overlain by the robust UG1 chromitite layer and UG1 pyroxenites.

(*b*) A distinctive texture characterizes almost the entire column extending for 350 m below the UG1 chromite. Spheroidal or embayed inclusions of partially resorbed plagioclase feldspar are found entrapped in abundance within orthopyroxene hosts. Rare grains of cumulus or xenocrystic feldspar are entrapped within some pyroxenites. Intragranular, cumulus and late intercumulus feldspar species thus exist within pyroxenites, as well as norites. Microprobe analysis shows that anorthite contents of included and non-included grains vary in sympathy, with the inclusions being generally more sodic.

(*c*) Sr_i ratios vary in an unpredictable manner from one sample to another. This indicates that the UG1FW unit could not have been the derivative of a single, homogeneous column of liquid within which phase or modal layering was controlled by purely physical parameters such as temperature, pressure, rhythmic nucleation or the sorting of crystals settling under gravity, or under the influence of currents.

(*d*) Sr_i ratios vary independently of stratigraphic height and petrographic features. Separate analysis of feldspar and pyroxene fractions shows that, within the same sample, isotopic signatures may be significantly different in these two fractions. Non-systematic whole-rock Sr_i variations can best be attributed to the feldspar population being a mixed one.

(*e*) The plotting of peak MMF ratios of orthopyroxenes of the UG1FW, UG1 and UG2 units, as determined by microprobe analysis, against whole-rock Sr_i ratios (Fig. 10) reveals that >80% of the available data points can be regressed. The derivation of this suite of rocks by some form of mixing between end members S ($Sr_i = 0.7054$; MMF = 0.78–0.79) and P ($Sr_i = 0.7068$; MMF = 0.82) is thus a viable hypothesis.

(*f*) Whole-rock major- and trace-element data indicate at least 8 sub-cycles between the MG4 and UG1 chromitite layers (Figs 3, 5 and 11). These sub-cycles are not demarcated by abrupt reversals of trends such as mark the transition from one full unit to another in the uppermost part of the Upper Critical Zone (as shown by Eales *et al.*, 1986). The pattern is, rather, one of gradational change to rocks of more, or of less, primitive type with stratigraphic height.

(*g*) The unit as a whole shows chemically evolved traits when compared with overlying cyclic units. It is depleted in Cr. Apart from a thin interval immediately above the MG4 chromitite layer, chromite is either absent or present as minute traces only, in contrast with its common occurrence as an accessory phase in norites and pyroxenites of the UG1, UG2, Merensky and Bastard units. The orthopyroxenes average 0.336% Cr_2O_3 (std. dev. = 0.045%; 43 samples; 393 analyses). By contrast, four union Section borehole intersections of the UG2 pyroxenite show average Cr_2O_3 levels to be 0.492%, 0.463%, 0.417% and 0.412% Cr_2O_3, respectively (averages drawn from 240 microprobe analyses). Similar Cr depletion is noted in Cameron's (1982, Table 2) data pertaining to the equivalent M unit in the eastern lobe of the complex. Moderate but consistent Ni depletion is also evident in our data insofar as 26 whole-rock pyroxenite samples yield an average $(Ni/MgO) \times 10^4$ ratio of 22.23 ± 0.80, within the range of 20.7–23.6. The average value is 24.0 ± 1.5 (range 22.8–27.2) within the overlying UG1 and UG2 units at Union Section, and 24.20 ± 0.85 (range 23.4–25.9) at Amandelbult Section. A further indication of chemically evolved traits is given by MMF ratios of the orthopyroxenes. A mean value of 0.798 for the entire

FIG. 9. Variations in $^{87}Sr/^{86}Sr$ at 2050 ± 25 (2 sigma) Ma (Sr_i) plotted against stratigraphic height for a 600 m section beneath the Bastard Unit (note changes of vertical scale above base of UG1 unit and below UG1FW unit). Filled circles—whole-rock data; triangles—plagioclase separates; squares—orthopyroxene separates. Stipple indicates pyroxenites, circles anorthosites, unshaded areas norites and cone symbols harzburgites of Pseudoreefs. Error bars are given at the 2 sigma level (see Appendix for details).

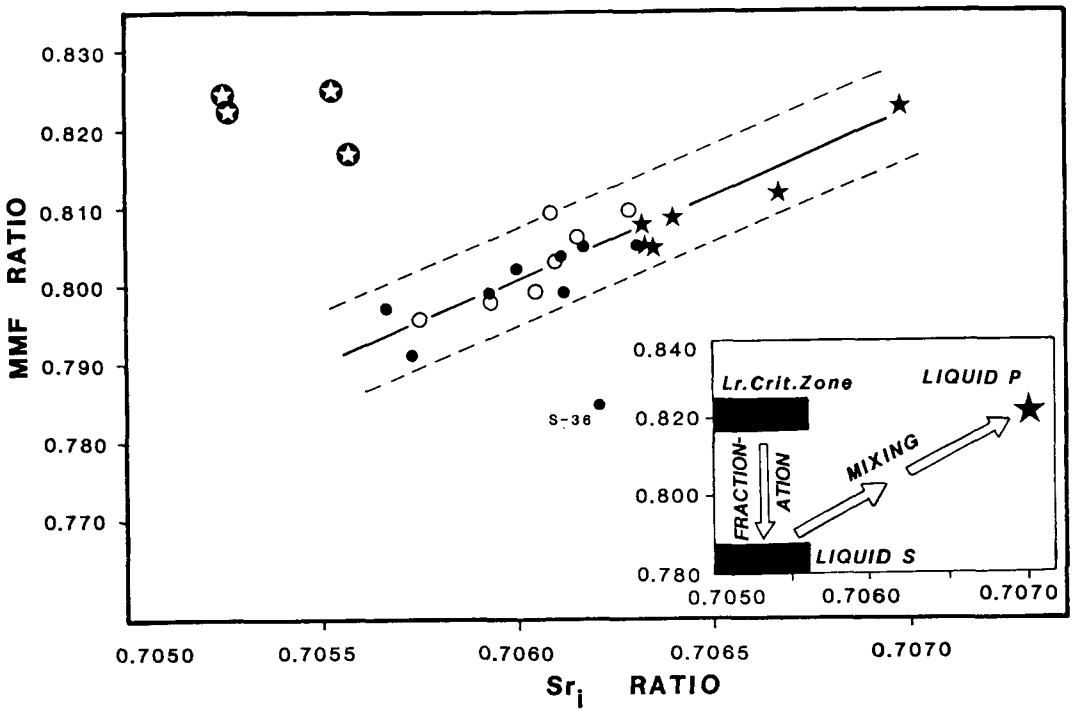

FIG. 10. Regression of peak MMF ratios detected by microprobe analysis of orthopyroxene population, against whole-rock Sr_i ratios for UG1FW norites (unfilled circles) and pyroxenites (filled circles), and UG1 and UG2 pyroxenites (stars). Also shown are 4 Lower Critical Zone pyroxenites (circled stars) and fractionated UG1FW unit pyroxenite sample S-36. Inset shows interpretation based on derivation of supernatant liquid S (liquid residuum of deeper-level cumulates) and subsequent mixing with primitive liquid P of UG1–UG2 lineage.

unit is suggestively lower than values of 0.822 ± 0.005, 0.817 ± 0.009, 0.814 ± 0.009 and 0.805 ± 0.007 determined in four separate intersections through the stratigraphically higher UG2 unit (24 samples; 240 analyses) at Union Section.

Discussion

Genetic models that are viable within the context of features (*a*)–(*g*) above are limited in number. Constraints imposed by the isotopic, petrographic, and gross chemical characteristics, and patterns of cryptic variations, leave little doubt about the operation of some process of mixing of a more primitive liquid with one bearing plagioclase in suspension. Hybridization apparently shifted the liquid composition into the primary phase volume of orthopyroxene, and led to compositional modification and partial resorption of the feldspar population. The muted internal cyclicity within the unit suggests that the process of hybridization was not a catastrophic event, but an ongoing one that waxed and waned in intensity. Accordingly, MMF, Ni/V and Cr/Co ratios define sub-cycles within the unit, without displaying a saw-tooth pattern, or marked discontinuities in trends.

The rôle which compositional convection (Tait *et al.*, 1984; Sparks *et al.*, 1984) might have played in influencing cryptic variations is uncertain. The concept recognises that changes in melt density, resulting from partial crystallization, may be more potent than temperature in promoting convection. Low-density residua may rise, in the earlier stages of crystallization, from a partially crystalline floor with high primary porosity, to be replaced by chemically undepleted melt drawn down into the crystal pile. Ostensibly, this provides a plausible mechanism for adcumulus growth. Such rocks should (*a*) exhibit extended growth of primocrysts into the void space that previously imparted high primary porosity, (*b*) show the most primitive chemical attributes where adcumulus traits are most extreme, and (*c*) yield fractionated residua in higher parts of the unit, to which low-density residua convect while phases

of high density are crystallizing. The general validity of this model is not under review here, but its applicability to the UG1FW unit is.

Our data on adcumulus bronzitites do not comply with the constraints. (*a*) Adcumulus growth by the mechanism of Tait *et al.* (1984) should yield overgrowth zones on pyroxene grains that are devoid of the abundant spheroidal feldspar inclusions. These inclusions are in reality as abundant close to grain margins as in cores of crystals in adcumulates (Fig. 2*d*). Rocks with more strongly orthocumulus affinities do display pyroxenes with marginal zones free of inclusions (Fig. 2*f*). This implies that adcumulus texture here is the result of compaction rather than grain enlargement. The fine grain size of the more extreme adcumulates of the UG1FW unit supports this argument. (*b*) If compositional convection governed the growth of adcumulates, samples with the highest MMF ratios should display the lowest degrees of residual porosity and, therefore, the lowest levels of incompatible elements (Henderson, 1968; Campbell. 1987). Conversely, entrapment of depleted residua should lower both whole-rock MMF ratios and, by reaction, those of ferromagnesian primocrysts (the trapped liquid shift of Barnes, 1986). Evidence here is unconvincing insofar as correlation coefficients between MMF ratios of pyroxenites (29 samples) and levels of incompatible elements Zr, Y and Ti are statistically weak (-0.36, -0.42 and -0.58, respectively). (*c*) Deposition of the UG1FW unit under a regime dominated by compositional convection, or crystal fractionation, should have led to accumulation of more evolved derivatives in the upper (noritic) half of the unit. Major- and trace-element whole-rock chemistry, and microprobe analysis of both pyroxenes and feldspars, prove conclusively that most of the upper half of the unit, although decidedly more feldspathic than the lower half, retains geochemically primitive traits. Averaged MMF ratios of norites are, in fact, higher than in pyroxenites. We conclude, therefore, that the totality of evidence requires periodic additions of primitive (Mg- and Cr-enriched) liquid to a resident column of evolved, supernatant liquid above the crystalline floor. Such a conclusion would accept the rising of low-density liquids, enriched in plagioclase component by compositional convection, and subsequent mixing with more primitive liquids.

The emplacement of an anorthositic (A-type) liquid within or beneath resident mafic (U-type) liquid, and subsequent mixing, has been cited as a fundamental process within the Bushveld complex (Irvine *et al.*, 1983; Sharpe, 1985; Harmer and Sharpe, 1985; Hatton, 1986). The A-type liquids of Sharpe (1985, Table 1) have higher Sr_i ratios (*c.* 0.7068) than U-type (*c.* 0.7030) and are, by definition, more feldspathic. The overall increase in Sr_i ratio, concomitant with a generalized increase in modal plagioclase with height in the UG1FW unit, therefore renders this a superficially attractive hypothesis. Other criteria refute the hypothesis. The upward increase in plagioclase in the UG1FW unit is accompanied by an increase in both MMF ratio and Cr content of the pyroxenes, which is the reverse of what an increasing proportion of A-type liquid would demand. Sr/Al_2O_3 ratios of Sharpe's putative A-type liquid (19.7×10^{-4}) are appreciably higher than ratios in U-type liquid (15.2×10^{-4}), whereas the noritic suite of the UG1FW unit maintains a remarkably constant ratio of $(14.8 \pm 0.7) \times 10^{-4}$ throughout. Cr/Ni and Cr/MgO ratios are, respectively, two and three times higher in U-type than in A-type liquids, but averaged values in the pyroxenitic and noritic suites of the UG1FW unit are indistinguishable (Cr/Ni of norites is 5.00 ± 0.33 and of pyroxenites 4.91 ± 0.50; Cr/MgO of norites is $(106 \pm 7) \times 10^{-4}$ and of pyroxenites $(108 \pm 11) \times 10^{-4}$). We find, therefore, no support for derivation of the norite–leuconorite suite by hybridization with discrete A-type liquid.

Some parallels may be drawn between the UG1FW unit and the Gabbronorite I–Olivine-bearing subzone I (OBZI)–Norite II sequence in the Lower Banded Series of the Stillwater complex (Barnes and Naldrett, 1986). In both, reversals of the normal fractionation trend are implicit in increased proportions of mafic phases, and enrichment in Mg, Ni and Cr. Rounded feldspar inclusions showing reversed zoning are enclosed in both (olivine in the OBZI and bronzite in the UG1FW unit) and imply a mixing of liquids resulting in partial resorption. Barnes and Naldrett postulate three end-member liquids—a primitive (P) liquid, an evolved resident liquid (G), and a feldspar-enriched (A) liquid yielded by high-pressure fractionation of P at depth. They argue that mixing took place within a thermal plume which spread laterally within resident G-type liquid, at some distance above the crystalline floor. Olivine bearing entrapped feldspar sank from the plume, through a column of resident G-type liquid before settling on the floor. Several paradoxes emerge when the Barnes–Naldrett model is applied to the UG1FW unit. Calling upon admixture with A-type liquid to account for the leucocratic nature of the upper part of the noritic suite does not explain the relative Cr- and Mg-enrichment characterizing the orthopyroxenes found there. By virtue of their evolution by extensive high-pressure fractionation of P-type liquids, A-type liquids

should be intrinsically Cr- and Mg-depleted. Furthermore, the composition of plagioclase inclusions becomes more sodic with height within subcycles of the UG1FW unit, in parallel with intercumulus plagioclase, while MMF ratios increase. The plume model offers no plausible reason for this.

Conclusions and synthesis

We adopt a model in which a hotter, more primitive liquid (P) is periodically added to and blended with a cooler, more evolved, supernatant liquid (S) resting upon the crystal pile. Sub-cycles developed within the unit include more primitive mafic cumulates deposited from hybrid liquids with a higher proportion of P component, whereas cumulates with more evolved traits reflect supernatant liquid fractions that experienced a lesser degree of rejuvenation, or evolved by subsequent fractionation. Extrapolation of the data embodied in Figs 5, 6 and 10 indicates the potential of these liquids to deposit cumulates with the following attributes:

Liquid S : Sr_i ratio *c.* 0.7054,
MMF of orthopyroxene *c.* 0.785,
Cr_2O_3 in pyroxene *c.* 0.25%,
Plagioclase *c.* An_{70},
Whole-rock Ni/V *c.* 2.9 and Cr/Co *c.* 20.

Liquid P : Sr_i ratio *c.* 0.7068,
MMF of orthopyroxene *c.* 0.82,
Cr_2O_3 in orthopyroxene *c.* 0.5%,
Plagioclase *c.* An_{81-85},
Whole-rock Ni/V *c.* 3.5 and Cr/Co *c.* 30.

The anorthositic tops of sub-cycles 7 and 8 (Fig. 5) introduce *c.* 3% anorthosite into the UG1FW unit. Our data offer no chemical or isotopic evidence to suggest that there was periodic influx of a discrete (A-type) magma from which these anorthosites crystallized. Even if the specific process that operated remains uncertain, we retain the view that liquids parental to the UG1FW unit anorthosites were generated within the magma chamber.

The more important variations in trends shown in Figs 3 and 5 are simplified in Fig. 11, to emphasize the cyclicity within the UG1FW unit, and a cartoon illustrating our synthesis is given in Fig. 12. Our synthesis to account for this cyclicity begins with (*a*) existence of a supernatant column of residual liquid, S, above the prevailing crystalline floor (Fig. 12*b*). Insofar as it was a liquid residuum generated during the separation of earlier cumulates, it was Cr-, Ni- and Mg-depleted, the Sr_i ratio was *c.* 0.7054 (Fig. 10), and it was nucleating sodic labradorite and Mg-poor bronzite in cotectic equilibrium. It is assumed that the liquid column was stratified, with the lowermost layer designated S representing the most dense liquid.

(*b*) Emplacement of a hot, primitive magma, P, with $Sr_i \geq 0.7068$ was then effected under conditions appropriate to jetting or fountaining (i.e. the intrusive liquid had a higher density than resident liquid; Campbell *et al.*, 1983; Campbell and Turner, 1986) rather than pluming. A hybrid layer consisting of P liquid, with entrained S liquid and suspended primocrysts, was formed immediately above the crystalline floor.

(*c*) Resorption, partial equilibration and reverse zoning of suspended, relict crystals inherited from the S liquid were initiated within the hybrid layer, and relative enrichment in the anorthite molecule was achieved in the small, severely corroded feldspar grains. A more limited temperature rise within the S liquid above the hybrid layer inhibited resorption and re-equilibration there, and plagioclase grains maintained a greater size and albite content than in the hotter hybrid layer.

(*d*) The addition of P liquid to S liquid in the hybrid layer shifted the system into the primary phase volume of bronzite (Fig. 12*c*), and subsequent nucleation and growth of bronzite primocrysts encapsulated relict feldspar grains. Compaction by sintering of the lower part of the crystallizing hybrid layer appears to have controlled the formation of adcumulate-textured pyroxenite with a low content of small, calcic feldspar inclusions. Above this, progressive crystallization of bronzite led to decline of the MMF ratio with height in some sub-cycles (1 and 2, Fig. 11). In others (sub-cycles 3 and 4 of Fig. 11), the P:S liquid ratio increased with time as more P liquid was injected, and earlier cumulates were covered by cumulates with increasingly higher Cr levels and MMF ratios (Fig. 12*d*). Reverse-zoned bronzite grains are commonly found here, but the earlier encapsulation of feldspar inclusions appears to have protected them from further reaction.

(*e*) All sub-cycles in the pyroxenite suite grade to Mg- and Cr-poor cumulates in their uppermost parts. This suggests fractionation through crystallization, but late-stage blending with evolved, supernatant (S) liquid overlying the hybrid layer was probably important (Fig. 12 *e–f*). The latter process would have been stimulated by the decline in density contrast between the two liquid layers, leading to breakdown of the interface as low-density residua migrated upwards by compositional convection during the separation of pyroxe-

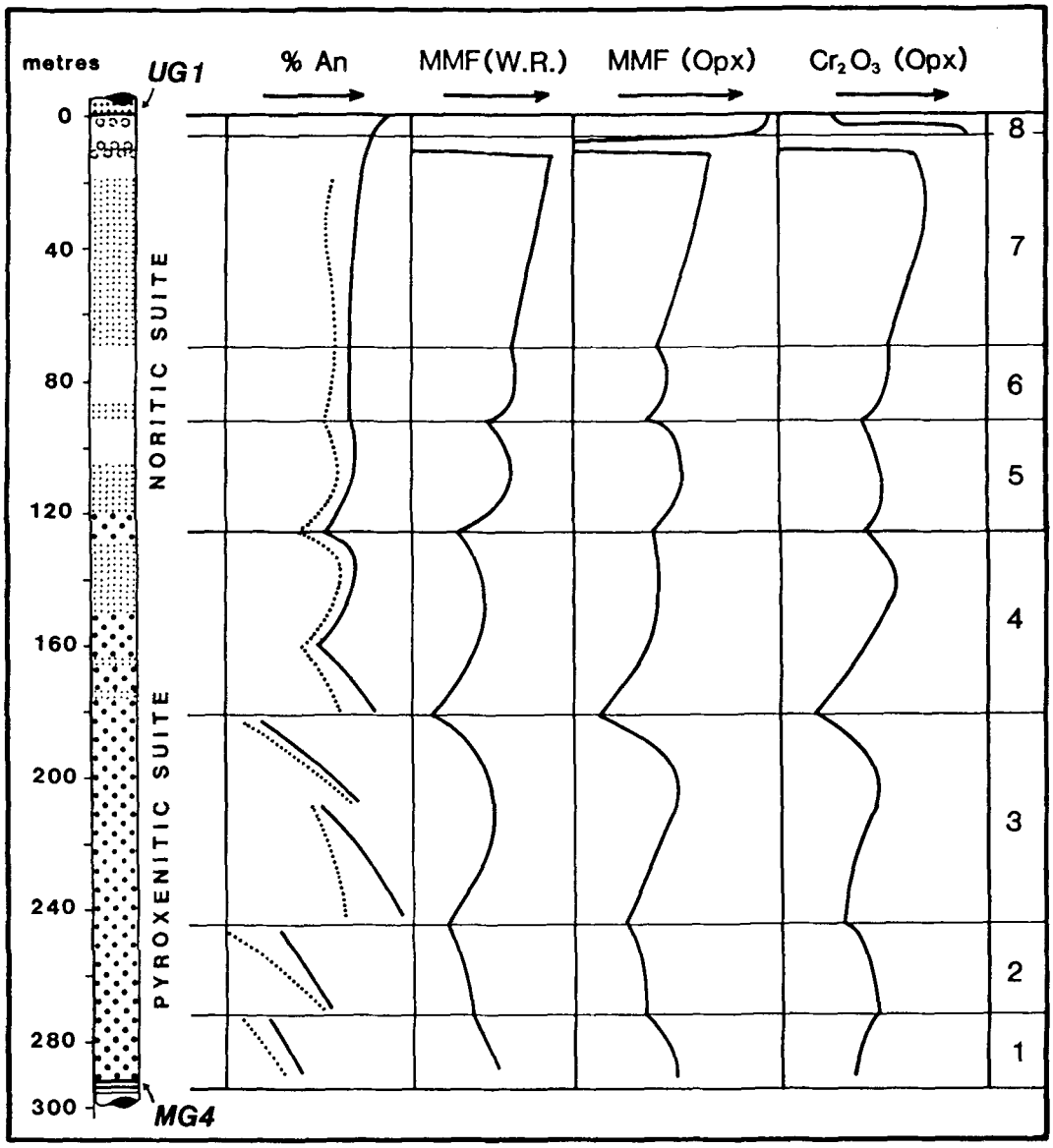

FIG. 11. Simplified representation of compositional trends depicted in Fig. 5, showing subdivision of sequence into sub-cycles 1–8. Dotted-line trends for feldspars represent inclusions in bronzite, and solid lines cumulus and intercumulus feldspars.

nites. The plagioclase inclusions trapped within pyroxene grains at this stage would, accordingly, have been relatively large, and sodic, reflecting their growth mainly in S-type liquid.

(*f*) Throughout accumulation of the pyroxenitic suite, the hybrid liquid was held within the primary phase volume of orthopyroxene by additions of P liquid, but there was substantial upward migration of low-density residua enriched in plagioclase components, as pyroxenite crystallized.

(*g*) Initiation of crystallization of intercumulus liquid lagged behind that of primocrysts. More calcic intercumulus feldspar would initially have nucleated at the base of the crystal pile, but concurrent compaction and reduction in primary porosity would have displaced sodic, intercumulus

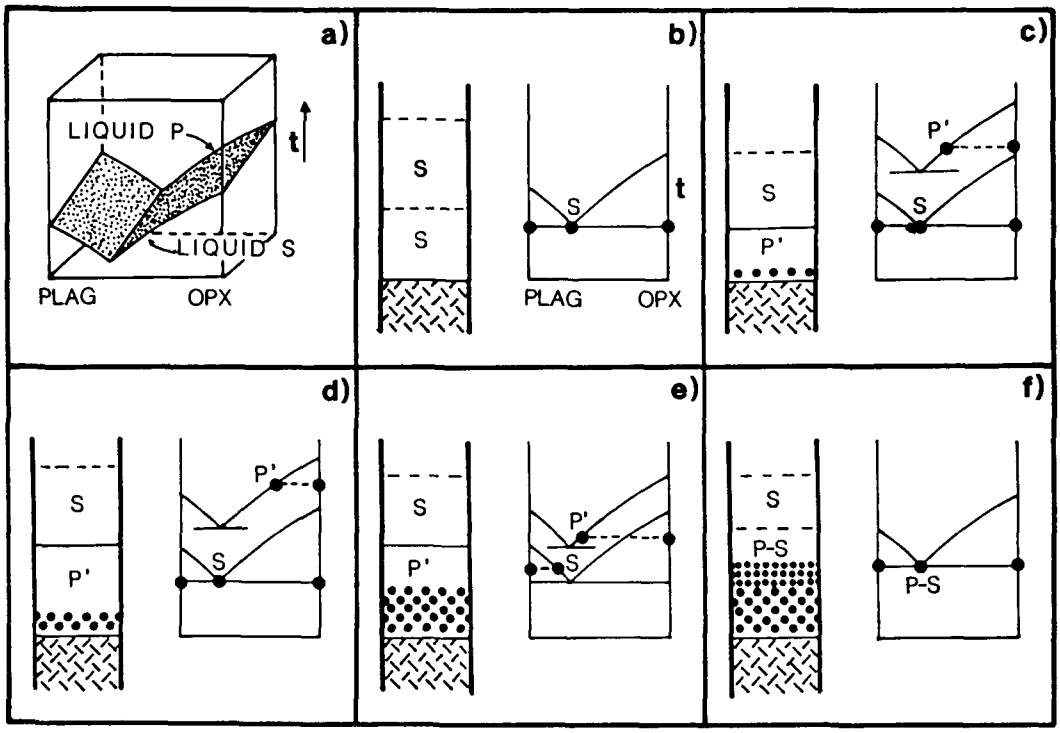

FIG. 12. Cartoon depicting sequence within an idealized sub-cycle. (*a*) Liquidus curves of evolved supernatant liquid S and more primitive inputs of liquid P. (*b*) Column of supernatant liquid S (probably stratified) resting upon existing floor (hatched). Qualitative phase diagram shows cotectic crystallization of plagioclase and orthopyroxene from liquid S. (*c*) Input of liquid P′ (P mixed with entrained S) beneath liquid layer S. P′ lies within primary phase volume of orthopyroxene; partially resorbed, relict plagioclase crystals suspended within liquid become entrapped within growing orthopyroxene grains. Preferential settling of orthopyroxene occurs within S, leaving it enriched in suspended plagioclase phenocrysts. Pyroxenite (stippled pattern) accumulates upon floor. (*d*) Continued input of P-type liquid leads to deposition of most magnesian orthopyroxene within sub-cycle. (*e*) Liquid P′ undergoes fractionation while liquid S (enriched in plagioclase due to settling of orthopyroxene) undergoes heating from below. Ultimately, liquid S enters primary phase volume of plagioclase as plagioclase is resorbed. (*f*) On subsequent cooling, advanced fractionation of low-volume residuum of P′ leads to conditions permitting mixing of P′ and S, forming hybrid P–S. Norite, leuconorite (finer stipple) and, in extreme cases, small volumes of anorthosite may be deposited from liquid P–S.

liquid residua upwards. Each subcycle therefore displays a trend towards sodic intercumulus feldspar with stratigraphic height (Fig. 11). Partitioning of Ca into late intercumulus clinopyroxene also has the potential to accelerate the shift towards sodic plagioclase (the augite effect of Morse, 1979).

(*h*) Periodic repetition of stages (*a*)–(*g*) above yielded sub-cycles 1–4 (Fig. 11). While the composition of successive pulses of intrusive P liquid remained sensibly constant (Figs 6, 7 and 10), the cumulative effects of repeated additions of P liquid to the system are evident. Fig. 11 shows that the starting compositions of both plagioclase inclusions and intercumulus plagioclase become systematically more calcic through sub-cycles 1 to 4.

(*i*) The slopes of the profiles depicting cryptic variations (Figs 5 and 11) are thus held to be a function of the volume and frequency of inputs of P-type liquid during the filling of the magma chamber. A low average volume and frequency of inputs per unit time resulted in sub-cycles of limited thickness (e.g. nos. 1 and 2 in Fig. 11) without pronounced reversals in the trend of cryptic variations; larger inputs of P liquid yielded thick sub-cycles within which significant increases in MMF ratio and Cr contents of orthopyroxene are seen (Fig. 11, sub-cycle 3).

(*j*) A significant change occurs within sub-cycle

4. Cumulus plagioclase joins the paragenesis ephemerally within thin layers of melanorite (7–10% Al_2O_3) at 175 m and 166 m depth; between 152 and 126 m the sequence becomes wholly noritic (11–16% Al_2O_3). The base of succeeding sub-cycle 5 exposes only 3 m of pyroxenite (5% Al_2O_3) before giving way to a noritic suite constituting the remainder of the UG1FW unit. The upper part of sub-cycle 4 thus marks the stage at which the hybrid liquid reached the bronzite–plagioclase cotectic. At this level, the decoupling of cryptic variations in bronzite and intercumulus plagioclase gives way to coupled variations between cumulus phases (see Fig. 11, sub-cycles 4–7). Several factors may have contributed towards the capacity of the hybrid liquid to crystallize primocrystal plagioclase. Upward movement and accumulation of low-density residua during protracted deposition of pyroxenites would have been important. Another factor might have been the preferential sinking of orthopyroxene out of the supernatant liquid layer S, followed by reheating of the layer as fresh influxes of primitive liquid were emplaced beneath it. This process would have had the capacity to generate a reservoir of liquid within the primary phase volume of plagioclase (Fig. 12 *e*).

(*k*) It is generally accepted (Campbell *et al.*, 1983; Sparks *et al.*, 1984) that the nucleation of plagioclase marks the evolutionary stage at which liquid residua will become more dense than the parent liquids. It is thus perhaps significant that the lowest MMF ratios in the UG1FW unit pyroxenites and lowest Cr contents of their orthopyroxenes, are encountered within the basal portion of sub-cycle 4, beneath the first norites (Figs 5 and 11). The implication is that fractionated residua no longer rose within the column above this point, but remained trapped as intercumulus liquid, or became ponded. Zonal decline of MMF ratios and Cr contents towards the margins of individual bronzite grains becomes the norm within the noritic suite. Oscillatory zoned feldspar primocrysts entangled within normally zoned (single-cycle) grains indicate the mixed nature of the population.

(*l*) A general trend towards increasing MMF ratios (whole-rock and microprobe data; Fig. 5 and 11) and increasing Cr in bronzite is maintained to within 20 m of the top of the UG1FW unit. Superimposed upon this is a muted cyclicity defining sub-cycles 5–7, suggesting minor, periodic influxes of primitive liquid. The apparent paradox of upward increase in MMF ratios and Cr levels in orthopyroxenes, as the sequence becomes more leucocratic, can be resolved in terms of mass balance. Additions of relatively small proportions of P liquid to a felsic liquid with a low content of ferromagnesian components would have increased MMF ratios without greatly increasing the absolute modal proportions of mafic phases.

(*m*) Sr_i ratios of norites and leuconorites (0.7058–0.7063) are within the range expected of a mixing of putative S liquids (*c.* 0.7054) and P liquids ($\geqslant$0.7068) in varying proportions. This range of values is well below that arising out of later emplacement of Main Zone liquids (*c.* 0.7087; Eales *et al.*, 1986) which might be equated with the A-type liquids of Sharpe, 1985). Fluctuations in Sr_i ratio are seen to be more conservative in norites (Fig. 9) than in pyroxenites because variations in the ratio S-type:P-type feldspars are more effectively buffered in norites, where feldspars are a major modal constituent.

(*n*) The band of leuconorite near the top of sub-cycle 7 (Fig. 5, 12–20 m) retains the chemical traits of the underlying norites, but the succeeding 6 m layer of anorthosite (32% Al_2O_3) at the top of sub-cycle 7 is strongly evolved. MMF ratios determined by both whole-rock and microprobe analysis of anorthosite samples drop to 0.62, Cr_2O_3 in orthopyroxene is <0.1%, and Ni/V, Cr/Co and Fe/Ti ratios are strongly depressed.

(*o*) The leuconorite at 4–6 m below the UG1 chromite (sub-cycle 8, Figs 5 and 11) shows higher MMF ratios and Cr contents of orthopyroxenes, and higher whole-rock Cr/Co ratios, than in sub-cycle 7 or in any underlying norites or pyroxenites of the UG1FW unit, but chromite does not yet appear as a phase. In the overlying 4 m anorthosite layer (the footwall of the UG1 chromitite layer) abundant chromite appears as disseminated grains, discontinuous layers, and pods. Microprobe data confirm that Cr contents are anomalously high for orthopyroxene found in anorthosites, and MMF ratios now match those of pyroxenes in the overlying UG1 unit. It is within the upper part of this anorthosite that the renowned system of anastomosing layers, and oblate spheroidal masses of chromitite that disrupt the layering (cf. Sampson, 1932; Lee, 1981; Viljoen *et al.*, 1986*a*) make their appearance. All these features point to interaction between a feldspathic residue at the top of the UG1FW unit, and the liquid parent of the overlying UG1 unit. The mixing of a chromiferous mafic liquid with feldspathic liquid has the potential to bring hybrids within the primary phase volume of Cr-spinel (Irvine *et al.*, 1983; Hatton and von Gruenewaldt, 1987) and the occurrence of the robust, if structurally complex, UG1 chromitite at this position is not in conflict with theory. We do not, however, subscribe to the view that the anorth-

ositic liquid need be derived as discrete injections of A-type liquid, as advocated by these authors. Indeed, the geochemical and isotopic data in this paper argue against the emplacement of a significant batch of A-type liquid at this level of the banded sequence.

Some conclusions of a broader nature emerge from this study. Firstly, Sr–isotope ratios are not reliable indices of either stratigraphic height or rock type within the complex, except in the broadest sense. Secondly, if the synthesis offered in this and two related papers (Eales *et al.*, 1986, 1988) is deemed valid, the broad thesis of Campbell *et al.* (1983) receives support. That is, the filling of a magma chamber to its full volume is accomplished in the early stages by injection of fresh magma pulses that intrude near the crystalline floor prevailing at that time. Jetting may be important. In the later stages, as within the uppermost part of the Critical Zone and the lower Main Zone, emplacement by pluming may become dominant. Thirdly, hybridization by partial resorption of earlier cumulates, or mingling of new liquids with older residual liquids may be a more general process than is commonly appreciated. It is only in specific sequences, as within the UG1FW unit, that this evidence is preserved in textural and chemical attributes.

Acknowledgements

Funding for this project was granted by the Foundation for Research Development of the C.S.I.R., for which our appreciation is recorded. The assistance of Claudia Schulte, Michelle Ellis, Andrea Wood and M. J. Aphane in sample preparation and analysis is acknowledged. Bernd Teigler is thanked for allowing us to incorporate his data on the Lower Critical Zone. Above all, the Management of R.P.M. Union Section Mine, and Dr Chris Lee, are thanked for allowing us access to mine workings, and for their goodwill and logistic support.

References

Barnes, S. J. (1986) *Contrib. Mineral. Petrol.* **93**, 524–31.

—— and Naldrett, A. J. (1986) *J. Petrol.* **27**, 791–825.

Cameron, E. N. (1964) In *Geology of some ore deposits in southern Africa,* **2**, Geol. Soc. S. Africa, 131–68.

—— (1982) *Econ. Geol.* **77**, 1307–27.

Campbell, I. H. (1987) *J. Geol.* **95**, 35–54.

—— and Turner, J. S. (1986) In *Short course in silicate melts* (C. M. Scarfe, ed.) Min. Assoc. Canada, 236–78.

—— Naldrett, A. J. and Barnes, S. J. (1983) *J. Petrol.* **24**, 133–65.

Coertze, F. J. (1958) *Geol. Soc. S. Africa Trans.* **61**, 387–92.

Eales, H. V. (1987) In *Evolution of chromium ore fields,* (C. W. Stowe, ed.) Van Nostrand Reinhold Co., New York, 144–68.

—— Marsh, J. S., Mitchell, A. A., de Klerk, W. J., Kruger, F. J. and Field, M. (1986) *Mineral. Mag.* **50**, 567–82.

—— Field, M., de Klerk, W. J. and Scoon, R. N. (1988) Ibid. **52**, 63–80.

Harmer, R. E. and Sharpe, M. R. (1985) *Econ. Geol.* **80**, 813–37.

Hatton, C. J. (1986) *Abstr. Geocongress Geol. Soc. S. Africa,* 595–98.

—— and von Gruenewaldt, G. (1987) In *In Evolution of chromium ore fields* (C. W. Stowe, ed.) Van Nostrand Reinhold Co., New York, 109–43.

Henderson, P. (1968) *Geochim. Cosmochim. Acta* **32**, 897–911.

Irvine, T. N. and Sharpe, M. R. (1982) *Carnegie Inst. Washington Ybk* **81**, 294–303.

Keith, D. W. and Todd, S. G. (1983) *Econ. Geol.* **78**, 1287–334.

Kruger, F. J. (1988) *Nuclear Active* **38**, 30–2.

Lee, C. A. (1981) *J. Geol. Soc. London,* **138**, 327–41.

Morse, S. A. (1979) *J. Geol.* **87**, 202–8.

Norrish, K. and Hutton, J. T. (1969) *Geochim. Cosmichim. Acta,* **33**, 431–53.

Sampson, E. (1932) *Econ. Geol.* **27**, 113–44.

Sharpe, M. R. (1985) *Nature,* **316**, 119–26.

Sparks, R. S. J., Huppert, H. E. and Turner, J. S. (1984) *Phil. Trans. Roy. Soc. London,* **A310**, 511–34.

Smith, J. V. (1974) *Feldspar Minerals,* **2.** Springer-Verlag, New York.

Tait, S. R., Huppert H. E. and Sparks, R. S. J. (1984) *Lithos,* **17**, 139–46.

Teigler, B. (1989) Ph.D. thesis, Rhodes University (in prep.).

Vermaak, C. F. (1976) *Econ. Geol.* **71**, 1270–98.

Viljoen, M. J., de Klerk, W. J., Coetzer, P. M., Hatch, N. P., Kinloch, E. and Peyerl, W. (1986a) in *Mineral deposits of Southern Africa* (C. R. Anhaeusser and S. Maske, Eds.) Geol. Soc. S. Africa, 1061–90.

—— Theron, J., Underwood, B., Walters, B. M., Weaver, J. and Peyerl, W. (1986b) Ibid. 1041–60.

Wager, L. R. and Brown, G. M. (1968) *Layered Igneous Rocks,* Oliver and Boyd, Edinburgh.

[*Manuscript received 12 July 1988; revised 11 July 1989.*]

Appendix–experimental methods

Sampling of the sequence was carried out along 20 Level Crosscut in the Spud Shaft Section of R.P.M. Union Section Mine, which affords excellent exposures with the layering dipping at 21° south-east. The MG4 chromitite horizon is here exposed at 1030 m below surface. Seventy-two samples of several kg each were taken at an average stratigraphic interval of 5m.

Isotope analysis. Sr and Rb concentrations were determined by isotope dilution mass spectrometry, and the $^{87}Sr/^{86}Sr$ ratio determined on the spiked sample. Approximately 100 mg of the sample powder was dissolved with ^{87}Rb and ^{84}Sr spikes in open Teflon beakers

using an $HF–HNO_3$ mixture on a hot plate. The sample was then dried and attacked with aqua regia to dissolve any precipitates. Cation exchange was carried out using 2.50M HCl and only the Sr fraction was collected. Sr was then loaded onto single outgassed Ta filaments using H_3PO_4; Rb was loaded onto double Ta filaments as a chloride without prior ion exchange separation. Total method blanks were less than 5 ng for Sr and *c.* 200 pg for Rb. In general, these amounts were not significant, with respect to the sample concentrations, and thus were largely ignored—with the exception of a Rb blank correction on the two plagioclase crystals of 3 mg, each from sample S-40. Both a VG-354 and a VG MM30 mass spectrometer were used to determine the isotopic ratios of Sr, whereas Rb was analysed using only the MM-30. During the period of this study, 19 replicates of the SRM-987 Sr standard were run on both machines. The results show that the machines are indistinguishable for that standard (VG 354—0.71022 ± 6 (2 std. dev.); MM-30—0.71025 ± 52). Replicate analyses of selected samples show that a one sigma precision of 1.5% in the ratio $^{87}Rb/^{86}Sr$ is a realistic estimate; uncertainties in $^{87}Sr/^{86}Sr$ present-day are 0.01% (1 sigma). Initial Sr ratios (Sr_i) are calculated at 2050 ± 25 Ma using the ^{87}Rb decay constant of 1.42×10^{-11} yr^{-1}. The total error quoted for Sr_i is based on analytical errors in $^{87}Rb/^{86}Sr$, $^{87}Sr/^{86}Sr$, and error in age, and was calculated with the isotope regression package, GEODATE, developed at the Council for Scientific and Industrial Research, Pretoria.

X-ray fluorescence spectrometry. Whole-rock analysis for major elements employed the fusion-disc technique of Norish and Hutton (1969). All samples were analysed in duplicate using a Philips PW 1410 XRF spectrometer and, where deemed necessary, analyses repeated in duplicate. Na_2O and trace elements were determined in 5g pressed powder briquettes, with corrections for background, spectral line interference, absorption and instrumental drift. All calibrations were made using a variety of USGS, NIMROC and other international standards. Determinations of Ti were run in quadruplicate for 15 samples of particular significance. All counting on spectral-line peaks for trace elements was fixed at 200secs, and 100secs for backgrounds. High precision for Sr and Rb was ensured by repeating the counting on peak for 400secs and 200secs on the background in a second run. The mean difference between samples in the two runs was 1.3ppm Sr for pyroxenites and 2.6 ppm for norites and leuconorites.

Electron microprobe. An automated JEOL CXA–733 electron microprobe was used for all mineral analyses, using well tested international standards and pure synthetic crystals for calibration. Most work was done with a defocussed 10μm beam.